Numerical study of flow maldistribution in plate heat exchangers used for evaporation process

PAWEŁ PLUSZKA
ARKADIUSZ PATRYK BRENK
ZIEMOWIT MIŁOSZ MALECHA[*]

Wrocław University of Science and Technology, Department of Cryogenic,
Aeronautic and Process Engineering, Wyb. Wyspiańskiego 27,
50-370 Wrocław, Poland

Abstract   Geometry of plate heat exchangers (PHE) is characterized by a complex net of narrow channels. It enhances turbulence and results in better heat transfer performance. Theoretically, larger number of channels (plates) should proportionally increase the PHE heat power capacity. In practice a nonuniform massflow distribution in consecutive flow channels can significantly deteriorate the overall heat exchange performance. The flow maldistribution is one of the most commonly reported exploitation problems and is present in PHE with and without phase-change flows. The presented paper investigates numerically a flow pattern in PHE with evaporation of R410A refrigerant. Various sizes of PHE are considered. The paper introduces a robust methodology to transform the complicated geometry of a real 3D PHE to its 2D representation. It results in orders of magnitude faster calculations and allows for fast evaluation of different geometrical changes of PHE and their effect on flow maldistribution.

Keywords: Plate heat exchanger; Flow maldistribution; Evaporation; OpenFOAM

Nomenclature

A –   area, m^2
C –   Lee model phase change coefficient

---

[*]Corresponding Author. Email: ziemowit.malecha@pwr.edu.pl

D	–	diameter of flow duct, m
DM	–	degree of maldistribution
g	–	gravitational acceleration, m/s^2
H	–	height, m
K	–	linear pressure drop coefficient
$\dot{m}$	–	mass flow, kg/s
MFR	–	mass flow ratio parameter
N	–	number of flow channels
p	–	pressure, Pa
L_{HT}	–	effective height of the plate, m
Re	–	Reynolds number
s	–	degree of flow non-uniformity
t	–	time, s
T	–	temperature, K
u	–	velocity, m/s
W	–	width of the flow channel, m
x	–	vapor quality, kg/kg

Greek symbols

α	–	volume fraction
Δp	–	pressure loss, Pa
ϵ	–	surface roughness, m
ρ	–	density, kg/m^3
ζ	–	local pressure drop coefficient
μ	–	dynamic viscosity of the fluid, Pa s
ν	–	kinetic viscosity of the fluid, m^2/s
ω	–	turbulence model variable

Subscripts

2D	–	two-dimensional
3D	–	three-dimensional
avg	–	average
baf	–	baffle
c	–	condensation
ch	–	channel
e	–	evaporation
eff	–	effective
ex	–	additional
h	–	header, hydraulic
i	–	ith instance
in	–	inlet
l	–	liquid
m	–	mixture
out	–	outlet
p	–	plates
sat	–	saturated
w	–	worst

v –   vapor
y –   vertical

Abbreviations

HVAC   –   heat ventilation and air conditioning
LPG   –   liquefied natural gas
PHE   –   plate heat exchanger

1   Introduction

Plate heat exchanger (PHE) is very efficient exchanger design character-ized by many advantages. Nonetheless, comparing to other design solu-tions, some undesirable phenomena may be significant for the PHE. The experimental and numerical findings of numerous authors are confirming the maldistribution problem in practically every type of heat exchanger design. The paper of Mueller *et al.* provides a comprehensive review of different causes provoking flow maldistribution [1]. The presence of mald-istribution may be created by mechanically-driven factors such as fouling, fabrication tolerances, bypass and poor header performance or be related to thermodynamic character of ongoing processes (two-phase instabilities, and heat-transfer induced as a consequence of changes in viscosity or den-sity) [2].

Considering PHEs, the maldistribution problem is reported in non-phase change applications [3,4,5,6,7] as well as in PHE condensers [8,9,10] or evaporators [11,12,13,14]. In the latter case, the phenomenon is especially undesirable, as it promotes uneven distribution of evaporating refrigerant mass flow across the consecutive PHE flowchannels. The dead zones in the furthest channels on the refrigerant's side may be created – the vapor may be trapped in certain part of the device causing a local dryout. Hence, the overall heat transfer efficiency of the exchanger would be significantly decreased. In different subcategories of plate heat exchangers the solutions to decrease the magnitude of maldistribution are mainly related to the inlet header design modification. In case of multi-stream plate fin exchangers, some solutions consider adding additional inlet baffles [15,16], rearranging configuration of channels [17], introducing internal two-phase distributor inside the exchanger [18]. For two-stream PHE, inlet distributor improve-ment is justified with results of Sterner *et al.* [12].

Flow maldistribution in two-stream PHE may be potentially improved by simply rearranging the inlet and outlet locations. It has been proven that when the streams are entering the devices from the opposite sides

of the PHE (Z-type), the mass flow across the flow channels is far more evenly distributed comparing to same-side openings (U-type) design [19]. However Z-type solution is not commonly preferred in heat, ventilation and air conditioning (HVAC) installations for some practical reasons, e.g., occupied space reduction, easier maintenance or conservation works and manufacturability cost decrease. Lin *et al.* [13] presented the differences in performance of a single two-plate flow channel considering a co-current or counter flow for evaporation process. They successfully captured the super-heat region by using infrared (IR) camera and quantified the evaporation heat transfer coefficients in each case.

The flow maldistribution can be minimized by geometrical optimization of PHE. An easiest to implement modification include an introduction of additional obstacles or separators in a collector (header) pipe of PHE. In practise, there is a large number of such modifications possible. To examine all of them experimentally may be very cumbersome, but it can be potentially achieved by means of fast and reliable numerical model.

The main objective of the present study was to create a robust methodology to transform a 3D geometry of real PHE to its 2D representation. It helped to develop a fast and accurate 2D model of PHE which could be used as a platform to investigate a flow behavior in PHE and optimize its performance.

The appropriate 2D representation of a real 3D PHE is crucial for numerical investigation of a wide parameter space of flow conditions and geometrical modification. In the author's previous paper [20] it was shown that a properly designed 3D numerical mesh of a typical PHE would consist of hundreds of millions of computational nodes. It is prohibitively too large for engineering applications, especially for calculations with a phase change and to investigate a wide range of parameter space. In the work [20] the reduction of the 3D model to its 2D representation was successfully carried out and confirmed by comparison with experimental results. Nevertheless, it considered only a single pair of plates (one channel). In the current studies a whole, multiplate, PHE is considered, and it is shown that crucial additions to the 2D model are necessary to correctly imitate the real geometry.

The currently proposed methodology of 2D reduction was based on preservation of a geometrical features and pressure drops. It resulted in orders of magnitude smaller computational mesh and allowed for an investigation of a wide range of geometrical and flow condition modifications.

Firstly, it was used to perform a number of calculations in a two-phase multi-plate PHE with evaporation processes included. A series of PHE with a different number of plates was considered to mark the beginning of the flow maldistribution in a function of number of plates. As a working fluid a refrigerant R-410A was used, which is widely utilized in HVAC systems.

In the second part a series of geometrical modifications was proposed to minimize the flow maldistribution. Especially, a larger number of plates was considered, to model more realistic PHE designs prone to more severe flow-maldistribution problems. The calculations in the second part were based on the air-water two-phase flow calculations without the vaporization process included. This simplification was crucial because the evaporization model needs considerably finer meshes and smaller time steps, what makes it impractical for investigation of larger geometries and different types of geometrical optimizations of PHE.

2   Numerical model and transformation to 2D geometry

Plate heat exchangers usually consists of several dozen plates, which are forming the flow channels when assembled together. The shape of the plates design is complex (see Fig. 1). It includes wavy shaping of plate's surface. That intensifies turbulence in the wall region, what promotes heat transfer magnitude. What is more, another important design feature has been applied in industrial manufacturing – the V-shape protrusion in vertical direction across the whole plate's height.

On the basis of geometrical characterization of single plate one may conclude that full three-dimensional numerical analysis of commercially utilized PHE is a tedious task. For single phase flow, with great support of high Performance computing machines (scientific clusters), the calculations may be feasibly performed in the acceptable amount of time. However, for the phase change processes, the computational effort is elevated, due to two main reasons: the requirement of heavily refined mesh, which enables to simulate the evaporation or condensation phenomena as well as introduction the new equations which are modeling the phase change process (there are various models available, varying with complexity). Hence, such computations would be unreasonable from engineering point of view, taking the time of months of computations. Due to rather practical and industrial aspect of examined phenomena we decided to transform the three-dimensional
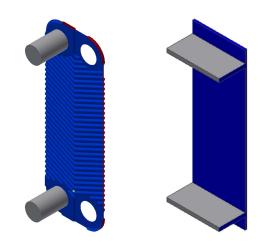
Figure 1: Comparison of real 3D geometry and its 2D representation.

real case into its simplified, but still consistent, two-dimensional numerical representation. To support this conclusion, we initially performed an attempt to assess the size of computational effort by meshing single 3D flow channel of real PHE. The study has been based on the work by Lin *et al.* [13]. The geometry dimensions were adjusted to preserve a consistency with a real PHE described in the mentioned paper (for dimensions reference see the Tab. 1). The sufficiently refined mesh of only one PHE flow channel consisted of a several millions of computational cells. Therefore, full-scale 3D phase change analysis would needed to be performed on the mesh of hundreds of millions of computational nodes. Even with help of high performance computers, such calculations would be extremely time-consuming. Therefore our next steps were concentrated only in the framework of two-dimensional domain.

As stated before, the 2D geometry was created based on [13]. Crucial dimensions are duct width, W_{ch}, depth, D, and longitudinal height of plates, L_{HT}. It has the same value as in the source paper [13] and is equal to 0.25 m. The main dimension in third axis has the same size as for the real PHE (0.102 m). If aforementioned dimensions are identically set for 2D geometry, it will assure the identical channel Reynolds number and heat transfer area for each plate. The Reynolds number in single channel is defined as function of inletting two-phase mass flow rate, $\dot{m}_{in}$, number of plates, N, and geometric dimensions of passage's hydraulic diameter, $D_{h,ch}$

Table 1: PHE dimensions used as reference [13].

Dimension	Value
Plate length	0.3 m
Plate width	0.102 m
Longitudinal distance between the stream ports	0.25 m
Plate thickness	0.0004 m
Amplitude of the chevron passage	0.002 m
Wave length	0.007 m
Chevron angle	65 °C
Hydraulic diameter of the chevron passage ($D_{h,ch}$)	0.004 m
Heat transfer area (plate projection, double sides)	0.051 m^2
Cross-section area of the single passage (A_{ch})	0.000204 m^2

and cross-sectional area, A_{ch}:

$$\text{Re}_h = \frac{\dfrac{\dot{m}_{in}}{N A_{ch}} D_{h,ch}}{\nu_l} \, , \tag{1}$$

where ν_l is a kinematic viscosity of liquid.

The headers as well as the collective horizontal channels were simplified to 2D representation preserving their inlet area. Hence, it implies that inlet velocity consistency was also satisfied. This requirement determined the height of the rectangular 2D inlet section, $H_{in,out}$, which is equal to 0.0074 m.

To reproduce the wavy (chevron) flow pattern inside the PHE channels without substantial increase of mesh size per plate, it was decided to introduce zero-thickness mixing baffles inside the 2D flow channel. They were placed alternately on both plates as shown on Fig. 2a. Applying these baffles allowed to reproduce a wavy pattern present in the complex trajectory of a fluid. It is one of critical aspects of 3D to 2D transition. Described approach was previously introduced and tested by author's in [20,21]. Amount of these baffles (26) was determined by analysis of the considered real 3D PHE geometry.
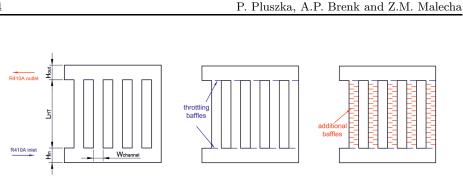
Figure 2: Schematic of characteristic features used in 2D geometry of PHE to model its 3D original: a) basic dimensions of 2D PHE; b) placement of throttling baffles; c) additional baffles modeling complexity of the flow of the 3D PHE.

To further reduce the mesh count it was assumed not to simulate the hot fluid side. Constant temperature boundary condition has been introduced on the plate surfaces. Such conditions might not reflect the actual real behavior of commercial PHE, but may still serve the purpose. Constant hot fluid temperature may be present in system if the mass flow of hot fluid is large enough to drive the temperature difference infinitesimally small. In the current study, which is intended to develop a robust numerical methodology, such assumption can be accepted as having a minimal impact on generalization of achieved results and conclusions.

An analysis of proposed 2D geometry when compared to its 3D original, shows a discrepancy in pressure balance across the PHE. Although the rectangular 2D header was modeled to preserve the inlet cross-section area, it did not conserve the same hydraulic diameter as for circular 3D header. Additionally, due to change of the shape of the inlets to the channels from a circular one (and localized in the middle of plates) to a rectangular one (see Fig. 1), there is a difference in local pressure drop as well.

A general idea to level these differences was to assure the same cumulative pressure losses in both geometries

$$2\Delta p_h^{3D} + \Delta p_{ch}^{3D} = 2\Delta p_h^{2D} + \Delta p_{ch}^{2D} \ , \tag{2}$$

where Δp_h^{3D} and Δp_h^{2D} are total pressure losses in the header of 3D geometry and its 2D representation respectively, Δp_{ch}^{3D} and Δp_{ch}^{2D} are total pressure losses in the channels of the 3D geometry and its 2D representation respectively. Rearranging and expanding the Eq. (2) gives

$$\frac{\overline{u}_{ch}^2 \rho}{2}\Big[\left(\zeta_{in}^{3D} - \zeta_{in}^{2D}\right) + \left(\zeta_{out}^{3D} - \zeta_{out}^{2D}\right)\Big] + 2\frac{\overline{u}_h^2 \rho}{2}\left(K_h^{3D} - K_h^{2D}\right) = 0 \ , \tag{3}$$

where ρ is the density, $\overline{u}$ is the average velocity of the fluid, ζ is the local pressure drop coefficient, K_h^{3D} and K_h^{2D} are the linear pressure losses in the header pipes of 3D and 2D geometry, which can be obtained by Darcy-Weisbach formula [22]

$$K_h^{3D/2D} = \begin{cases} \dfrac{64}{\mathrm{Re}} & \text{for} \quad \mathrm{Re}_h < 2300 \ , \\[2ex] 0.11 \left(\dfrac{68}{\mathrm{Re}} + \dfrac{\varepsilon}{D_{eff}} \right)^{\frac{1}{4}} & \text{for} \quad \mathrm{Re}_h \geq 2300 \ , \end{cases} \tag{4}$$

where $D_{eff} = 64/96 D_h$ is modified hydraulic diameter of the duct, suitable for 2D rectangular ducts [22]. For three-dimensional case D_{eff} is equal to D_h.

Comparing the 3D and 2D geometries, there is a higher linear pressure drop in the header pipes (bottom and top collector of 2D PHE) but lower local losses at the inlets and outlets of the PHE channels in case of 2D geometry. It can be noticed that $\Delta p_h^{3D} < \Delta p_h^{2D}$ and $\Delta p_{ch}^{3D} > \Delta p_{ch}^{2D}$.

In general $\zeta_{in}^{3D} \neq \zeta_{in}^{2D}$, $\zeta_{out}^{3D} \neq \zeta_{out}^{2D}$ and $K_h^{3D} \neq K_h^{2D}$ and to fulfill the Eq. (3) an extra pressure loss must be included to fulfill the equations:

$$\begin{aligned} \zeta_{in}^{3D} - \zeta_{in}^{2D} + \zeta_{in,ex}^{2D} &= 0 \ , \\ \zeta_{out}^{3D} - \zeta_{out}^{2D} + \zeta_{out,ex}^{2D} &= 0 \ , \\ K_h^{3D} - K_h^{2D} + K_{h,ex}^{2D} &= 0 \ . \end{aligned} \tag{5}$$

The determination of the additional pressure loss coefficients need at inlet and outlet in 2D geometry was performed based on the recently published work of Brenk *et al.* [23]. The single-phase flow methodology presented in the mentioned paper has been transferred directly to the present paper.

The local loss coefficients $\zeta_{in,ex}^{2D}$ and $\zeta_{out,ex}^{2D}$ are unknown and needed to be evaluated numerically. For this purpose, two models of PHE were created and each of them contained only two flow passages (four plates). The first geometry was based on 3D PHE model and had a circular tube header (Figs. 3a and 3b), and the second model was based on 2D PHE and had a rectangular duct header (Fig. 3c and 3d). To assure accurate estimation, both models were created as three-dimensional, and each mesh contained over 30 millions of computational cells. Calculation of the local loss coefficients were done based on numerical results of pressure and velocity field on dark surfaces in Fig. 3 and calculated using $\zeta = \frac{2\Delta p}{\overline{u}^2 \rho}$.

The aforementioned extra 2D pressure losses: $\zeta_{in,ex}^{2D}$, $\zeta_{out,ex}^{2D}$, and $K_{k,ex}^{2D}$ were included in the 2D geometry as properly designed local losses in a form

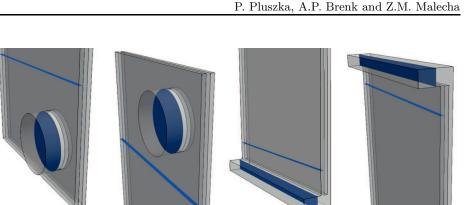(a) Inlet 3D (b) Outlet 3D (c) Inlet 2D (d) Outlet 2D

Figure 3: Views of the circular and rectangular inlet/outlet channels used for numerical estimation of local loss coefficients by means of 3D incompressible calculations. The dark surfaces marks the measurements cross-sections.

of additional throttling baffles at the every inlet and outlet the PHE channels (Fig. 3b) to preserve the same pressure loss balance between original 3D geometry ant its 2D representation. The additional linear pressure loss in the header $K_{h,ex}^{2D}$ was calculated using Darcy-Weisbach formula [22] and was directly included in the local losses coefficients. The final sizes of the throttling baffles for the inlet and outlet channels are shown in Tab. 2. Exemplary inlet throttling baffle is presented in Fig. 4.
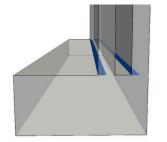

Figure 4: Bottom baffle 50% [23].

Table 2: Flow maldistribution expressed as average absolute deviation s.

Variable	Re = 50	Re = 250
$\zeta_{in,ex}$	11.5	2.95
$h_{in,baf}$	0.00122 mm	0.00083 m
$\zeta_{out,ex}$	17.1	4.31
$h_{out,baf}$	0.00122 mm	0.00079 mm

To decrease the flow maldistribution phenomena the redesign of the inlet header channel by introducing different type of baffles has been proposed. The main function is to force the fluid stream to inflow into channels with more uniformly distributed mass flow. It should be mentioned that all the configurations may be potentially applied in mass industrial production,

because the changes proposed are not critical from the manufacturability point of view. The investigated proposals have been collected in Fig. 5. Figure 5a presents the horizontal baffle, sized as half of the PHE length, which has been placed in the symmetry plane of the header's geometry. The flow is supposed to split out on two equal mass flow streams. Figure 5b is reproducing the previous design with addition of closure presented at the end of the upper surface of the baffle. Last proposal (Fig. 5c) is also a modification of the first option. The vertical coordinate of the baffle is increased – it separates the internal header volume into the two parts equal to 20% and 80% of the total volume.

case 1 – half-length opened symmetrical baffle

case 2 – half-length closed symmetrical baffle

case 3 – half-length opened non-symmetrical baffle

Figure 5: Schemes of inlet header modifications: a) horizontal baffle placed symmetrically, b) same baffle but closed at the end c) horizontal baffle placed asymmetrically (80% of header's height).

In the proposed modifications, the inletting stream of refrigerant is expected to get separated and delivered to different regions of PHE. The number of baffles, their placement and horizontal dimensions can be further optimized to provide significantly larger (than evenly distributed baffles) mass flow to the rear flow channels of the PHE.

3 Mathematical model description

In order to solve the described flow an open-source OpenFOAM 16.12+ software was employed [24]. The main solver used was *interCondensatingEvaporatingFoam* [25] which includes Lee phase change model [26]. The solver is designed for simulations of two incompressible, non-isothermal immiscible fluids which may exchange mass during phase-change process. The momentum, energy, and other fluid properties are derived for a the two-fluid

mixture:

$$\rho_m = \alpha_l \rho_l + \alpha_v \rho_v \ , \qquad (6)$$

$$\mu_m = \alpha_l \mu_l + \alpha_v \mu_v \ , \qquad (7)$$

where α_l and α_v are volume fractions of liquid and vapor respectively and $\alpha_l + \alpha_v = 1$ [26]. Volumetric fraction of vapor phase has been calculated based on empirical void fraction formula from Baroczy [27]

$$\alpha_v = \left[\left(\frac{1-x}{x} \right)^{0.74} \left(\frac{\rho_v}{\rho_l} \right)^{0.65} \left(\frac{\mu_l}{\mu_v} \right)^{0.13} \right]^{-1} \ . \qquad (8)$$

The momentum and energy equations for the mixture flow are defined in the mixture model as follows [27,29]:

$$\frac{\partial}{\partial t}(\rho_m \boldsymbol{u}_m) + \nabla \cdot (\rho_m \boldsymbol{u}_m \boldsymbol{u}_m) = -\nabla p + \nabla \cdot \mu_m \nabla \boldsymbol{u}_m + \rho_m \boldsymbol{g} \ . \qquad (9)$$

The evaporation process is modeled by the Lee model [26], which has been widely used in various phase-change processes [30]. There are couple of simplifications introduced in the model. The phase change occurs in constant pressure and a quasi-thermo equilibrium state. Moreover, the mass transfer mainly depends on saturation temperature and the interfacial temperature between phases is equal to saturation temperature as well. The rates of mass exchange between liquid and vapor phases are added to the continuity equation:

$$\frac{\partial(\rho_v \, \alpha_v)}{\partial t} + \nabla(\rho_v \, u_v \, \alpha_v) = R_e - R_c \ , \qquad (10)$$

$$\frac{\partial(\rho_l \, \alpha_l)}{\partial t} + \nabla(\rho_l \, u_l \, \alpha_l) = R_c - R_e \ . \qquad (11)$$

The rates of mass exchanged are defined as follows:

$$R_c = C_c \, \rho_v \, \alpha_v \, (T_{sat} - T) \,, \qquad R_e = 0 \qquad \text{for} \qquad T < T_{sat} \,, \qquad (12)$$

$$R_e = C_e \, \rho_l \, \alpha_l \, (T - T_{sat}) \,, \qquad R_c = 0 \qquad \text{for} \qquad T > T_{sat} \,, \qquad (13)$$

where ρ, α, and T stands for density, phase volume fraction and temperature respectively. The indexes v and l refer to vapor and liquid states. Parameters C_c and C_e are numerical constants. High values of these parameters assure fast calculations. It was stated in [30] that large values of C_c and C_e may cause issues with simulation convergence, while too small

values could be a reason of significant deviation between the interfacial temperature and the saturation temperature. An intense sensitivity analysis regarding coefficients C_c and C_e has been done in terms of our case geometry. It was reported that the results were coherent with conformity error up to 10%. It showed that these parameters had a minor influence on the overall two-phase flow behavior. Therefore to maintain a high speed of solver these parameters were both set to 10.

4   Numerical model

The PHE geometry used for the evaporation process is characterized by the 15 mesh elements included across the 0.002 m width flow channel. Additional 3 levels of wall refinement has been introduced, to preserve the wall treatment with good resolution. For inlet and outlet header the mesh count in cross direction amounts to 70, with 2 levels of wall refinements. The size of computational domain equals approx. 0.6, 1.1, and 2.2 million elements for number of 10, 20, and 40 flow channels, respectively. Figure 6 provides a general overview of the computational domain. Both throttling and wavy
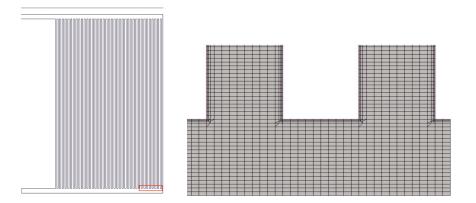

Figure 6: Domain (left) and mesh close-up (right) for the geometry of 40 flow channels.

baffles has been configured as thermodynamically inert by setting temperature boundary condition of *zeroGradient*. Hence, they influence only to the flow pattern, without interfering with temperature field. As stated before, the hot side behavior of the exchanger has been represented by the prescription of constant boundary temperature on the surfaces of plates. The two-phase flow inlet composition is corresponding to the inlet vapor quality

of refrigerant of $x = 0.385$ which for given R410A conditions results in volumetric vapor fraction equal to $\alpha_v = 0.84$. Such level of vapor entering the evaporator may occur during severe exploitation or break-down of cooling systems in, e.g., air conditioning. It is assumed that inletting refrigerant's void fraction is perfectly uniformed across the inlet section. The whole internal domain has been initialized from the aforementioned void fraction value. The saturation temperature has been defined as 274.25 K (1.1 °C). Thermodynamic properties such as density, conductivity and viscosity has been acquired using the open-source CoolProp material libraries [31]. The mass flow has been adjusted in each case to conserve the Reynolds number of 250 in the flow channel. It has been calculated according to Eq. (1). For all of the simulations the k-ω turbulence model has been utilized. The velocity profile has been assumed as turbulent (power law). Special treatment has been applied for the boundary conditions of kinetic turbulent energy and rate of its dissipation. The authors took advantage of work published by Lewandowski *et al.* [32], in which the novel analytic approach of turbulent boundary conditions for k-ϵ model has been derived. The transient PISO (pressure-implicit with splittings of operators) [eeded] solver has been utilized with maximum Courant number of 0.35. This requirement defined timestep per iteration as per 10^{-5} s for Re = 50 cases and one order of magnitude less for the Re = 250 simulations.

5 Results of the calculations

Together with investigation the massflow distribution, parallel study of the PHE outlet region has been conducted. From experimental findings it is known, that the flow maldistribution impacts negatively on the vapor parameters on the outlet. For this purpose, the liquid fraction and the superheated temperature extracted from the outlet section has been presented in Fig. 7.

According to the diagrams, the negative influence has not been detected. The liquid volume fraction curve is approximately the same for all the cases. The complete evaporation takes place for different time coordinates, but after 4 s of simulation all PHEs are confirmed to step into the superheating conditions. The values has been extracted from the outlet section of PHE. After approx. 4 s of simulation all PHEs are confirmed to step into the superheating conditions. Further calculations confirm reaching a steady state of the system. Thus, all results shown in this chapter has been extracted
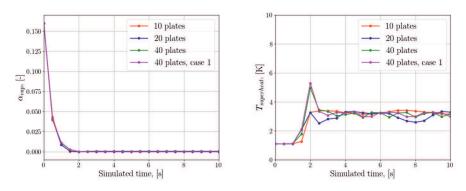
for the simulated time of 10 s.

Figure 7: Comparison of investigated PHE cases in terms of the volumetric liquid fraction and superheated temperature at the PHE outlet.

Another possible reason why the curves are very close to each other is the fact, that the expected observations may not be visible due to two reasons: yet not large enough simulated PHE or the constant temperature wall boundary condition, which helps to evaporate the refrigerant more evenly. It should be mentioned that in real life industrial situation in U-type PHE similar flow maldistribution would occur on the hot side fluid. Hence, adding the second medium and modeling the full thermal interaction between the fluids should contribute to revealing the true impact of maldistribution on outletting vapor's parameters. Figure 8 presents the results of three cases considering presence of 10, 20, and 40 flow channels respectively. At first the baseline PHE geometries (without any modifications) have been simulated. Each case was simulated for total flow time of 10 s. On the right side figure presents the distribution of the liquid fraction indicating full evaporation state at the outlet of exchanger. The subplots on the left show the mass flow variations in consecutive flow channels. They had been extracted from the middle cross cross section of the PHE.

The figures presents the two-phase fluid composition extracted from the middle height of plate heat exchanger. At this coordinate nearly all liquid has evaporated into the vapor phase. The flow maldistribution inside the PHE channels may be observed in each case – with tendency to increase its magnitude as the number of plates increases. As the investigated exchanger is U-type PHE, bigger mass flow is transported in the region closer to inlet and outlet openings.
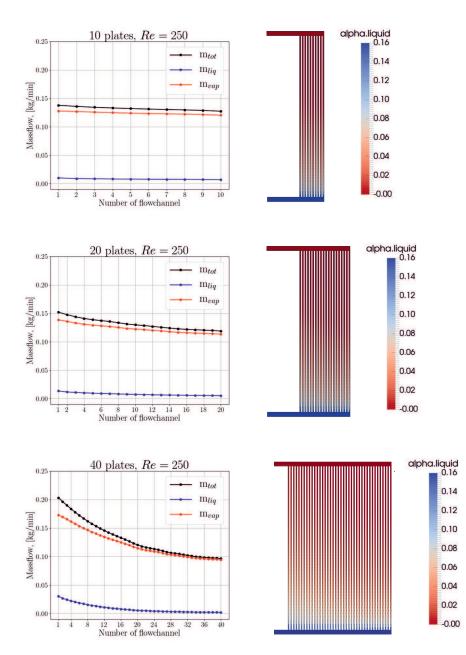
Figure 8: Distribution of two-phase R410A flow (Re = 250) across the PHE flow channels. Stabilized solution for simulated time of 10 s. Half-height PHE section.
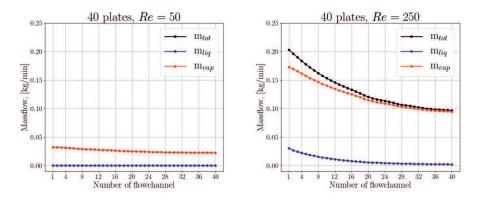
Figure 9: Comparison of mass flow distribution for the 40 plates PHE cases between the systems characterized by Reynolds number Re = 50 (left) and Re = 250 (right). Section taken from the half-height of exchanger.

Figure 9 presents the comparison of 40 plates geometry for two Reynolds number of 50 and 250. The flow intensity is reported to be the main factor driving the maldistribution. Depending on the refrigerant mass flow transported through the exchanger, the complex multiple plate geometry may react with the desired distribution of fluid flow inside the flow channels (for low Reynolds number) or perform inefficiently when the flow channel Reynolds number is higher. As Re = 250 is more commonly applied in the PHEs, the next steps in optimization were tested only for this value, as it was assumed that solutions improving the flow characterized by Re = 250 are also beneficial for lower Reynolds numbers.

Very heavy computation demands made the calculations for a larger number of plates impractical and out of scope of present studies. It is clearly visible that the effect of flow maldistribution has been successfully captured using the proposed numerical approach. For the largest PHE considered (40 plates) the total refrigerant mass flow in first flow channel is approximately as twice big as in the last one. The figure indicates that there is significant need to optimize the mass flow distribution.

As a consequence of mass flow non-uniformity, it may be observed that the upper right region of PHE (the furthest from the inlet) is working in superheated conditions. The amount of liquid refrigerant provided to rear channels is insufficient. This drives the tendency to evaporate entire liquid portion before it reaches the outlet header. The phenomenon has been illustrated in Fig. 10. In the most complex case considered (40 plates,
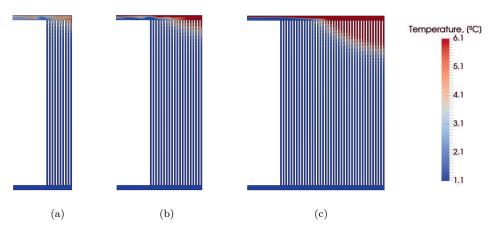
Figure 10: Temperature distribution in the exchanger for: a) 10, b) 20, c) 40 flow channels. Stabilized solution for simulated time of 10 s.

see Fig. 10c, significant region of PHE has been superheated with more that 5 K. It is expected to observe enlarged superheat region for the bigger PHEs.

Evaluation of three concepts to decrease magnitude of maldistribution effect has been presented collectively in Figs. 11. Baseline case of *no baffle* has been added to perform convenient comparison between cases. Distributions of two main outputs have been investigated: mass flows of vapor and liquid refrigerant phase. All data has been extracted for one-forth and three-forth of the PHE height. The purpose for it was to assess the flow pattern in two levels in which the vapor mass quality differs extensively.

Considering case 1 geometry, similar solution has been previously applied in single-phase flow model providing significant improvement of flow non-uniformity [23]. On top of that, using case 1 alike baffle for two-phase separated flow (without phase change) was also confirmed to decrease the maldistribution (for the tested case high ratio of phases' densities was present). For evaporation process symmetrical baffle shows very similar behavior to referential *no baffle* case. Almost no significant change in mass flow pattern is noticed, only in the region of baffle's outlet small local mass flow rise can be observed. Two next cases have been proposed as possible ways to improve the inefficiency of solution of case 1. Depending on PHE manufacturing feasibility one can either close baffle (case 2) at its end or shift its vertical position inside inlet header (case 3). In both cases sig-
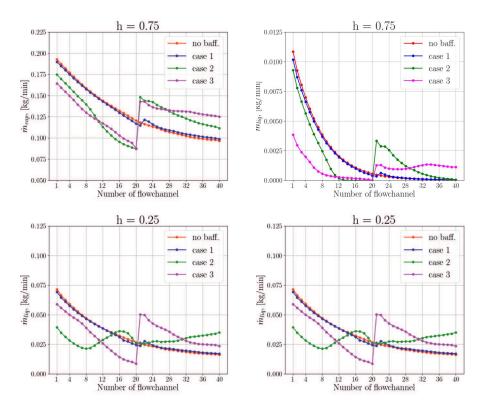
Figure 11: Distribution of R410A vapor (left) an liquid (right) mass flows across the PHE flow channels for different baffle modifications (including baseline). Stabilized solution for simulated time of 10 s. Section taken from the 75% and 25% of the PHE height.

nificant change is spotted. In general, latter variants are providing more fluid to the rear part of PHE, causing decrease of mass flow supplied to the frontal flow channels. Sudden rise of refrigerant mass flow may be spotted in the region of baffle's outlet. What is more additional baffle in the inlet header has separated the exchanger into two parts, the decreasing trend of mass flow provided to consecutive channels remained similar. Despite latter point it can be concluded that overall cases 2 and 3 performed better comparing to baseline and case 1 simulations.

Possible explanation of differences between cases may be revealed by investigation of the velocity field near the end of the separating baffle (Fig. 12). For case 1 recirculation areas created nearby the baffle edge may have contributed to formation of flow pattern very close to the base-

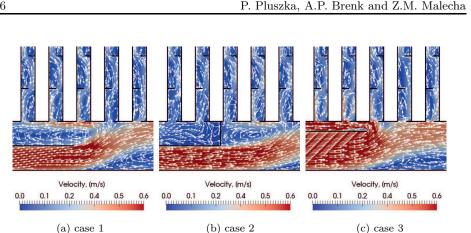(a) case 1   (b) case 2   (c) case 3

Figure 12: Local flow pattern near baffle's end.

line one. Closure of the baffle (Fig. 12b) caused perfect separation of fluid streams helped to supply refrigerant to flowchannels' inlets in more uniform degree. For case 3 portion of bottom stream is returning back into top part of header. This phenomenon is driven by enlarged pressure drop in first channels. Variation of baffle vertical position may be applied to reach uniform flow distribution across the PHE.

In terms of superheated region decrease (Fig. 13), relatively smallest improvement may be seen for case 1. Closure of baffle (case 2) provides visible improvement. The top region of PHE is performing more evenly. Last variant improves the flow on the intermediate level between aforementioned previous cases. It decreased the superheat magnitude in top right corner of PHE, however created a new extensive superheat area in the central flow channels.

To discuss the characteristic of the flow distribution it was convenient to introduce a parameter called the *mass flow ratio* (MFR), which was calculated for each channel according to the formula

$$\text{MFR}_i = \frac{\dot{m}_i}{\dot{m}_{avg}} = \frac{\dot{u}_{y,i}}{\dot{u}_{y,avg}} \ , \tag{14}$$

where $\dot{m}_i$ represent the mass flow rate in ith channel, and $\dot{m}_{avg}$ is the average mass flow rate of refrigerant. Next criterial parameter introduced was the degree of flow non-uniformity, s. Similar coefficient was used in [33] to represent results of flow maldistribution study. It was derived as an

(a) no baffle   (b) case 1

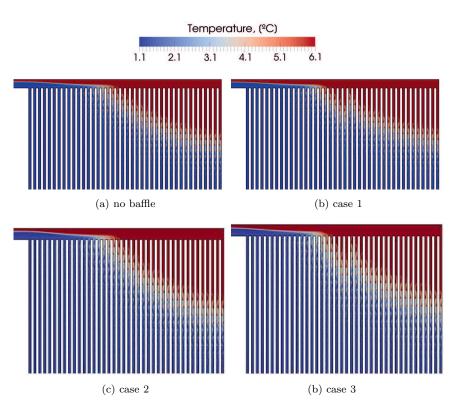(c) case 2   (b) case 3

Figure 13: Influence of inlet header modifications on the temperature field in PHE.

average absolute deviation s calculated as follows:

$$s = \frac{1}{N} \sum_{i=1}^{N} |\text{MFR}_i - \text{MFR}_{avg}| \ , \tag{15}$$

where average mass flow ratio MFR_{avg} equals 1, and channel number N is varying between the 10 and 40 plates. Here $s = 0$ denotes ideal flow distribution. Based on Eq. (15), the parameter for the degree of maldistribution DM was defined as

$$\text{DM} = 1 - \frac{s}{s_w} \ , \tag{16}$$

where s_w is the worst possible maldistribution calculated using Eq. (15) with the assumption that the whole flow escapes the PHE through the first channel. The value of DM changes from 0 to 1, where 1 means a uniform mass flow in every channel (no maldistribution). MFR and DM numbers

Table 3: Flow maldistribution assessment.

Case	s	DM
no baff	0.1608	0.917
1	0.1578	0.919
2	0.1393	0.929
3	0.1112	0.943

are used to evaluate and compare results for different modifications within easy to obtain criterial numbers. Both parameters have been extracted from the half-height section of the PHE. Summarized results of s and DM have been presented in Tab. 3. The flow maldistribution improvement assessed by degree of flow non-uniformity can be as big as 31% for case 3, which is proving the biggest profit out of tested concepts. Coherent trend can be observed for the degree of maldistribution whereas all baffle modifications are closer to ideal condition of DM = 1 comparing to the baseline geometry.

6   Conclusions

The presented work has been focused on developing maximally efficient numerical methodology, capable of dealing with phase change processes in complicated geometries like the plate heat exchangers. The transformation of real 3D geometry into its 2D representation is a key feature to reduce the size of computational mesh. Having incorporated simplified mathematical model of evaporation and condensation, the authors have investigated the flow maldistribution phenomenon. It is worth emphasizing that the current methodology may deliver directional results and by means of evaluating different baffle options indicates the optimal way to achieve more efficient design of PHE.

Application of horizontal baffle in refrigerant inlet header may contribute to significant decrease of the flow maldistribution phenomenon. It has been concluded that three main factors decide about the success of baffle concept: vertical coordinate of fixation, length of baffle, and number of baffles in the channel. Broader study is required to investigate the conjoined influence of each baffle. Closing the baffle is reported to be improving the situation. However, applying this solution in the industrial process may

not be always feasible from the manufacturability point of view.

There are a few directions for development of current numerical approach. They have been listed as follows:

- After establishing a robust approach for modeling the cold side of the PHE, it is convenient to introduce the second fluid into the computational domain and consider conjoined behavior of two interacting fluids. That would definitely improve the quality of numerical predictions (better description of heat and fluid-flow physics) as well as allow to deliver results closer to the typical industrial cases). For preliminary evaluations the second, hot medium may be considered to be the water.

- Current approach of setting perfectly uniform phase composition fractions at the inlet of the PHE may be a next feature to modify in order to simulate real-life thermal processes. For relatively large vapor qualities, the flow inletting into the header may become stratified or annular. It has a potential to modify the current mass flow distribution. The two-phase flow inlet characteristics will undoubtedly affect the results especially when combined with the separating effect of the horizontal baffles.

- Having working phase-change numerical model one may switch the initial refrigerant to different fluid. Very interesting proposal is *liquefied natural gas* (LNG), which numerical investigations are part of the current research of the authors.

- Introducing LNG to the model will naturally provide additional physics to the model related to the hot side. In processes of cryogenic liquids regasification it is crucial to maintain the temperature of hot medium above the freezing point. It is a limiting boundary below which the solidification takes place. For the plate heat exchanger type the solidification is extremely dangerous because it may swiftly block the narrow flow channels between the plates and significantly deteriorate the performance of the device. This is the main motivation of expanding the LNG version of numerical model by the liquid-solid phase change on the water side.

Received 10 January 2019

References

[1] MUELLER A. C., CHIOU J.P.: *Review of various types of flow maldistribution in heat exchangers.* Heat Transfer Eng. **9**(1988), 2, 36–50. DOI:10.1080/01457638808939664.

[2] PACIO J.C., DORAO C.A.: *A study of the effect of flow maldistribution on heat transfer performance in evaporators.* Nucl. Eng. Des. **240**(2010), 11, 3868–3877. DOI:10.1016/j.nucengdes.2010.09.004.

[3] CHOWDHURY K., SARANGI S.: *Effect of flow maldistribution on multipassage heat exchanger performance.* Heat Transfer Eng. **6**(1985), 4, 45–54. DOI:10.1080/01457638508939638

[4] FLEMING R.B.: *The effect of flow distribution in parallel channels of counterflow heat exchangers.* In: Advances in Cryogenic Engineering (K.D. Timmerhaus, Ed.). Springer, Boston 1967, 352–362.

[5] JUNG J., JEONG S.: *Effect of flow mal-distribution on effective NTU in multichannel counter-flow heat exchanger of single body.* Cryogenics **47**(2007), 4, 232–242. DOI:10.1016/j.cryogenics.2007.01.004.

[6] PAWAR N., MAURYA R.S.: *Flow maldistribution in a simplified plate heat exchanger model-a numerical study.* In: Appl. Mech. and Mater. **110**(2012), Trans Tech Publ, 2529–2536.

[7] KLUGMANN M., DABROWSKI P., MIKIELEWICZ D.: *Pressure drop related to flow maldistribution in a model minichannel plate heat exchanger.* Arch. Thermodyn. **39**(2018), 2, 123–146. DOI: 10.1515/aoter-2018-0015.

[8] WANG Z.-Z., ZHAO Z.-N.: *Analysis of performance of steam condensation heat transfer and pressure drop in plate condensers.* Heat Transfer Eng. **14**(1993), 4, 32–41. DOI:10.1080/01457639308939809.

[9] WANG L., CHRISTENSEN R., SUNDEN B.: *An experimental investigation of steam condensation in plate heat exchangers.* Int. J. of Heat Exch. **1**(2000), 2, 125–150.

[10] BOBBILI P.R., SUNDEN B.: *Steam condensation in parallel channels of plate heat exchangers.* In Proc. ASME Int. Mechanical Engineering Cong. Expo.: Vol. 7, Fluid Flow, Heat Transfer and Thermal Systems; Pts. A and B, 2010, 851–857. DOI:10.1115/IMECE2010-39974.

[11] Vist S., Pettersen J.: *Two-phase flow distribution in compact heat exchanger manifolds.* Exp. Therm. Fluid Sci. **28**(2004), 2, 209–215. DOI: 10.1016/S0894-1777(03)00041-4.

[12] Sterner D., Sunden B.: *Performance of Plate Heat Exchangers for Evaporation of Ammonia.* Heat Transfer Eng.**27**(2006), 5, 45–55. DOI:49510.1080/01457630600559611.

[13] Lin Y.-H., Li G.-C., Yang C.-Y.: *An experimental observation of the effect of flow direction for evaporation heat transfer in plate heat exchanger.* Appl. Therm. Eng. **88**(2015), 425–432. DOI:10.1016/j.applthermaleng.2014. 11.074.

[14] Jensen J.K., Kaernl M.R., Ommen T.S., Brix W., Reinholdt L., Elmee-gard B.: *Effect of liquid/vapour maldistribution on the performance of plate heat exchanger evaporators.* In: Proc. 24th IIR Int. Cong. of Refrigeration, 2015.

[15] Wen J., Li Y., Wang S., Zhou A.: *Experimental investigation of header configuration improvement in plate–fin heat exchanger.* Appl. Therm. Eng. **27**(2007), 11, 1761–1770. DOI:10.1016/j.applthermaleng.2007.01.004.

[16] Raul A., Bhasme B.N., Maurya R.S.: *A numerical investigation of fluid flow maldistribution in inlet header configuration of plate fin heat exchanger.* Energy Procedia **90**(2016), 267–275. DOI:10.1016/j.egypro.2016.11.194.

[17] Peng X., Liu Z., Qiu C., Tan J.: *Effect of inlet flow maldistribution on the passage arrangement design of multi-stream plate-fin heat exchanger.* Appl. Therm. Eng. **103**(2016), 67–76. DOI:10.1016/j.applthermaleng.2016.04.072.

[18] Yuan P., Jiang G.B., He Y.L., Yi X.L., Tao W.Q.: *Experimental study on the performance of a novel structure for two-phase flow distribution in parallel vertical channels.* Int. J. Multiphase Flow **53**(2013), 65–74. DOI:10.1016/j.ijmultiphaseflow.2012.05.006.

[19] Srihari N., Rao B.P., Sunden B., Das S.K.: *Transient response of plate heat exchangers considering effect of flow maldistribution.* Int. J. Heat Mass Transfer **48**(2005), 15, 3231–3243. DOI:10.1016/j.ijheatmasstransfer.2005.02.032.

[20] Malecha Z., Płuszka P., Brenk A.: *Numerical investigation of cryogen regasification in a plate heat exchanger.* IOP Conf. Ser. Mater. Sci. Eng. **278**(2017), 1, 012063. DOI:10.1088/1757-899X/278/1/012063.

[21] Malecha Z.M., Malecha K.: *Numerical analysis of mixing under low and high frequency pulsations at serpentine micromixers.* Chem. Process. Eng. **35**(2014), 3, 369–385.

[22] White F.M.: *Fluid Mechanics* (4th Edn.). McGraw-Hill, 2014.

[23] Brenk A., Płuszka P., Malecha Z.: Numerical study of flow maldistribution in multi-plate heat exchangers based on robust 2D model. Energies **11**(2018), 11, 3121. DOI:10.3390/en11113121.

[24] Weller H.G., Tabor G., Jasak H., Fureby C.: *A tensorial approach to computational continuum mechanics using object-oriented techniques.* Comput. Phys. **12**(1998), 6, 620–631. DOI:10.1063/1.168744.

[25] *The Open Source CFD Toolbox User Guide*, 2014.

[26] LEE W.H.: *A pressure iteration scheme for two-phase flow modeling.* In: Multiphase Transport: Fundamentals, Reactor Safety, Applications (N. Veziroglu, Ed.) . Hemisphere Publishing, Washington, DC 1980.

[27] VAN WACHEM B.G.M., ALMSTEDT A.E.: *Methods for multiphase computational fluid dynamics.* Chem. Eng. J. **96**(2003), 1, 81–88. DOI:10.1016/j.cej.2003.08.025.

[28] BAROCZY C.J.: *Correlation of liquid fraction in two-phase flow with applicatio to liquid metals.* Chem. Eng. Prog. Symp. Ser. **57**(1965), 61, 179–191.

[29] RANADE V.V.: *Computational Flow Modeling for Chemical Reactor Engineering*: Vol. 5 (1st Edn.). Academic Press, San Diego 2001.

[30] DE SCHEPPER S.C.K., HEYNDERICKX G.J., MARIN G.B.: *Modeling the evaporation of a hydrocarbon feedstock in the convection section of a steam cracker.* Comput. Chem. Eng. **33**(2009), 1, 122–132. DOI:10.1016/j.compchemeng.2008.07.013.

[31] BELL I.H., WRONSKI J., QUOILIN S., LEMORT V.: *Pure and pseudo-pure fluid thermophysical property evaluation and the open-source thermophysical property library CoolProp.* Ind. Eng. Chem. Res. **6**(2014), 53, 2498–2508. DOI:10.1021/ie4033999.

[32] LEWANDOWSKI M.T., PŁUSZKA P., POZORSKI J.: *Numerical investigation of cryogen re-gasification in a plate heat exchanger.* Int. J. Numer. Methods Heat Fluid Flow, DOI:10.1108/HFF-02-2017-0078.

[33] ZHANG ZH., LI Y.-ZH., XU Q.: *Experimental research on flow maldistribution in plate-fin heat exchangers.* Chin. J. Chem. Eng. **12**(2004), 1, 7–13.